

SHORT COMMUNICATION

Metasomatic monazite growth as a result of apatite-fluid interactions: U-Pb dating of monazite in the Siilinjärvi glimmerite-carbonatite complex, Finland



SEPPO KARVINEN^{1*}, KATHRYN CUTTS², HUGH O'BRIEN²,
CHRISTOPH BEIER¹ AND AKU HEINONEN².

¹ *Department of Geosciences and Geography, Research programme of Geology and Geophysics (GeoHel), University of Helsinki, Gustaf Hällströmin katu 2, PO Box 64, 00014 Helsinki, Finland*

² *Geological Survey of Finland, PO Box 96, 02151 Espoo, Finland*

Abstract

Monazite U-Pb results obtained for a calcite carbonatite sample from the Siilinjärvi glimmerite-carbonatite complex yields a lower concordia intercept age of 1760 ± 17 Ma (2σ uncertainty, $n = 50$). This age is inconsistent with the magmatic emplacement age (ca. 2610 Ma) of the complex based on published zircon U-Pb ages. The conspicuous and systematic spatial relationship among large apatite grains and fine-grained monazite and apatite indicates monazite formation through fluid-mediated dissolution-precipitation processes. The monazite dating result presented here supports the prior interpretation that this monazite is post-magmatic in origin and provides a minimum age for the fluid-mediated dissolution-precipitation processes in the Siilinjärvi complex.

Keywords: monazite, apatite, U-Pb geochronology, metasomatic, dissolution-precipitation, metamorphism, Archean, Svecofennian

*Corresponding author (e-mail: seppo.karvinen@helsinki.fi)

Editorial handling: Jussi S. Heinonen (email: jussi.heinonen@abo.fi)

1. Introduction

Monazite is a mineral group of light rare earth element phosphates [(LREE)PO₄] named according to the dominant cation [e.g., monazite-(Ce), CePO₄]. Monazite group minerals often incorporate Th and U, allowing their radiogenic ages to be determined using the (Th-)U-Pb isotope system (e.g., Williams et al. 2007 and references therein; Schoene 2014). Monazite has a Pb closure temperature comparable to that of zircon (> 900 °C, Cherniak et al. 2004) and as such, is robust against resetting of the system due to volume diffusion. Metasomatism, the process of alteration of a rock by a fluid in disequilibrium, involves addition or removal of chemical components (e.g., Yardley 2013). Interaction with hydrothermal fluids may reset the isotope system below closure temperatures by fluid-mediated dissolution-precipitation processes in monazite-fluid reactions (e.g., Budzyń 2011; Williams et al. 2011) or to the formation of new monazite in apatite-fluid reactions (Harlov et al. 2005; Harlov 2015).

The Siilinjärvi glimmerite-carbonatite complex, located in eastern Finland (Puustinen 1971; O'Brien et al. 2015), was likely emplaced at 2610 ± 4 Ma, based on zircon U-Pb dating (an unpublished age of O. Kouvo, 1984, concordia shown in O'Brien et al. 2015). Similar ages have been reported by other studies (Rukhlov & Bell 2010 and references therein). Other isotope systems in other minerals yield considerably younger ages (2030–1785 Ma, K-Ar in phlogopite; Puustinen 1972; ~1770 Ma, Rb-Sr isochron, phlogopite; Tichomirowa et al. 2006) that have been interpreted to represent metamorphic overprint during or after the Svecofennian orogeny (e.g., Hölttä & Heilimo 2017) which took place at 1920–1770 Ma (e.g., Korsman et al. 1999; Lahtinen et al. 2005, 2018).

Monazite has been reported in the glimmerite-carbonatite rocks found within the Siilinjärvi complex (Al-Ani 2013; O'Brien et al. 2015; Karvinen et al. 2024) but no age determinations have been published. Karvinen et al. (2024) studied the petrography and chemical composition of

apatite within the complex and found that monazite is petrographically associated with large apatite grains and interpreted the monazite to be the metasomatic product of apatite-fluid dissolution-precipitation processes (e.g., Harlov et al. 2005). In this study, we dated the monazite previously studied by Karvinen et al. (2024) utilizing in situ U-Pb analysis to investigate the age of the monazite and present an interpretation of their formation via metasomatic processes.

2. Geological background

The Siilinjärvi glimmerite-carbonatite complex is located in the Karelia province (Nironen 2017) to the east of the NW-trending Raahe-Ladoga suture zone that roughly marks the Archean-Proterozoic boundary (see Kohonen et al. 2021). The complex consists primarily of glimmerite (phlogopite-rock) that is crosscut by sub-vertical calcite carbonatite dikes that represent only 1.4 or 2.3 % of the total rock volume, in the Särkijärvi main and Saarinen satellite pits, respectively (O'Brien et al. 2015). The petrology of the complex is presented in detail in Puustinen (1971) and O'Brien et al. (2015). The complex has likely been affected by several deformation events during and possibly before the Svecofennian orogeny (O'Brien et al. 2015). The complex is located within a roughly N-trending shear zone (Lukkarinen 2008) and it shows signs of deformation from macroscale, evident as the irregular, bifurcating Y-shaped plan section of the complex down to microscale as recrystallized calcite and fractured apatite grains and kinked phlogopite (e.g., Sartori et al. 2022; Karvinen et al. 2024).

3. Samples and methods

3.1 Scanning electron microscopy (SEM)

Two petrographical sections (thin and thick, 30 and 100 μm , respectively) of sample SAA4 (sheared calcite carbonatite, Saarinen satellite pit; see Karvinen et al. (2024) for detailed petrography) were studied using Hitachi SU3900 scanning electron microscope (SEM) with back scattered electron (BSE) images at the Geological Survey of Finland, Espoo, Finland. The samples were scanned with electron dispersive X-ray spectrometry (EDS, X-Max 20 mm² silicon drift detector) with an acceleration voltage and probe current of 20 kV and 1 nA, respectively. The scans were followed by automated classification by AzTEC software (Oxford Instruments) that detects phases and classifies grains according to their size, shape, and composition. The method provides non-standardized chemical compositions that are normalized to 100 wt.% that are considered semi-quantitative. Monazite grains were then imaged to study possible zonation and to target U-Pb geochronology spots and were found to be unzoned in high contrast BSE images (Fig. 1; Electronic Appendix A, Karvinen et al. 2026).

3.2 Monazite U-Pb geochronology

A total of 59 analyses from 49 monazite grains were analyzed for U-Pb isotopes in situ from two polished sections representing a single sample (SAA4; Electronic Appendix A) with laser ablation single-collector inductively coupled plasma mass spectrometry (LA-SC-ICP-MS) at the Geological Survey of Finland, Espoo, Finland. The setup consists of a Teledyne Photon Machines Analyte Excite+ 193 nm laser coupled with a Nu Instruments AttoM single-collector mass spectrometer. A detailed description of the method can be found in Molnár et al. (2018). The following masses were measured: ²⁰²Hg, ²⁰⁴Pb, ²⁰⁶Pb, ²⁰⁷Pb, ²⁰⁸Pb, ²³²Th, ²³⁸U. ²³⁵U was calculated from the ²³⁸U

signal, using the natural ²³⁸U/²³⁵U ratio of 137.88. Monazite were pre-ablated for 1 s with a 20 μm beam, followed by a 20-s washout period before gas background was analyzed for 20 s followed by ablation for 40 s. The analysis beam diameter was 15 μm , repetition rate and fluence were 5 Hz and 1.09 J/cm², respectively. The unknown analyses were bracketed with analyses of both in-house (A49, 1874 \pm 3 Ma; A1326, 2635 \pm 2 Ma; Hölttä et al. 2000) and external reference monazites (TS, 910.42 \pm 0.34 Ma, Budzyń et al. 2021a; Vermilion, 2666.5 \pm 3.0 Ma, Mazoz et al. 2024; Thompson Mine, 1766 \pm 0.6 Ma, Williams et al. 1996). Standards were run after every 15 sample analyses. The data was reduced in Lolite (Paton et al. 2011) version 4 using the VizualAge UComPbine data reduction scheme (DRS, Petrus & Kamber 2012; Chew et al. 2014) with TS as the primary reference material. The analyses were not corrected for common Pb, see Electronic Appendix B for details. The DRS plots the signal selection live on a concordia diagram that allows the selection of a concordant portion of the signal, in case of heterogenous concordance within an analysis. The readers are referred to Petrus & Kamper (2012) for an in-depth explanation of this approach. External uncertainties were propagated into all age calculations and uncertainties are reported at the 2 σ level. Reference monazite yielded the expected concordia ages, within uncertainty. Results for reference monazite are reported in Electronic Appendix B. The sample results are presented below in a Tera-Wasserburg concordia plot (Fig. 2). All results can be found in Electronic Appendix C. All geochronology figures and calculations were created with IsoplotR (Vermeesch 2018).

4. Results

All analyzed grains are classified as monazite-(Ce) (later “monazite”), based on the prevalence of Ce over other lanthanides in EDS analyses (25.8 \pm 2.65 wt.% Ce, semi-quantitative; Electronic Appendix C). Monazite crystal habits range from individual, anhedral to subhedral grains to grain

aggregates (Fig. 1). The U content is highly variable, but <10 ppm in most analyses ($n = 47$, 84 %, Fig. 3). Thorium is more abundant (median 765 ppm) but likewise shows a wide range among analyses (42–7990 ppm). Consequently, Th/U is on median 121, from 3 to 2177. Three analyses were of poor quality and were discarded during data reduction.

In Tera-Wasserburg concordia space, most analyses are discordant, plotting slightly above the concordia curve or forming a discordia towards higher $^{207}\text{Pb}/^{206}\text{Pb}$ and lower $^{238}\text{U}/^{206}\text{Pb}$. Individual single-spot age outliers were excluded from date calculations (empty ellipses Fig. 2). The remaining analyses yield a Tera-Wasserburg concordia lower intercept date of 1760 ± 17 Ma (2σ uncertainty, $n = 50$, Fig. 2), calculated using model 3 in IsoplotR, fitted by a discordia line using a modified maximum likelihood algorithm that accounts for overdispersion by an added geological variance term (Vermeesch 2018).

5. Discussion

5.1 Evaluation and interpretation of the results

The monazite age result of ca. 1760 Ma indicates closure of Pb system in monazite over 800 Myr after the ca. 2610 Ma crystallization of zircon in the Siilinjärvi glimmerite-carbonatite complex, which is regarded as the magmatic age (e.g., Rukhlov & Bell 2010; O'Brien et al. 2015). The result presented above is, to the authors' knowledge, the first published dating result of monazite from the Siilinjärvi glimmerite-carbonatite complex. Were the monazite analyzed in this study comagmatic with zircon, they should yield a similar U-Pb date, as zircon and monazite have comparable, high closure temperatures for Pb (≥ 900 °C; e.g., Cherniak et al. 2004) yet none of the analyses do. An alternative interpretation for the 1760 ± 17 Ma age is that the monazite is primary (i.e., 2610 Ma) and was completely overprinted by fluid-mediated

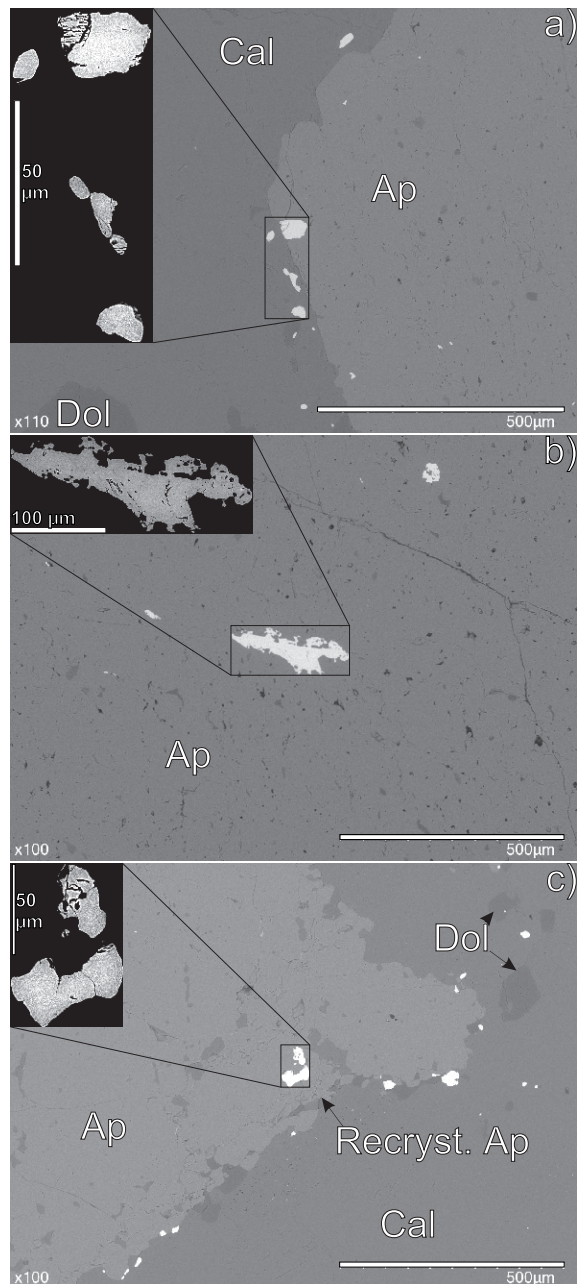


Figure 1. Backscattered electron (BSE) images of monazite textures (white in BSE), with high-contrast close-up insets that show that the monazite is unzoned. Large apatite (Ap) is surrounded by groundmass calcite (Cal) with minor dolomite (Dol). Monazite is typically found on the grain boundaries of large apatite grains (a, c), as subhedral grains, associated with recrystallized, fine-grained apatite (Recryst. Ap; c) or anhedral or subhedral as inclusions within apatite (b). The highest analyzed U content (480 ppm) is found in analyses 77a,b from the anhedral monazite within apatite (b).

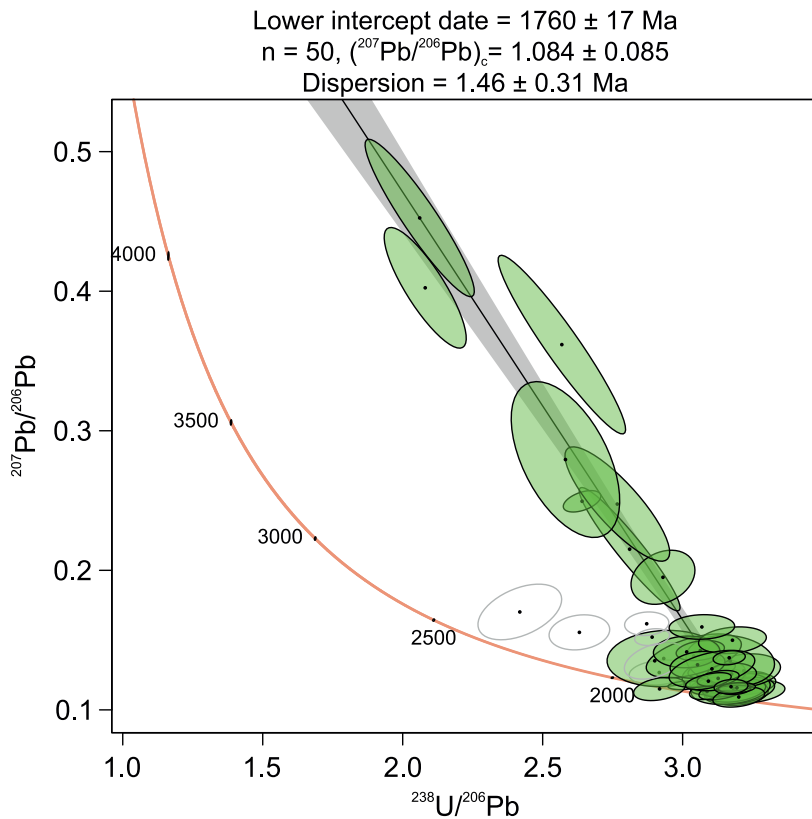


Figure 2. Monazite U-Pb results plotted in Tera-Wasserburg space with a lower concordia intercept at 1760 ± 17 Ma (2σ), calculated with IsoplotR (Vermeesch, 2018) using discordia model 3 (see text). Empty ellipses denote analyses not used in the discordia calculation ($n = 6$) as they were determined to be outliers based on their calculated concordia intercept ages. Age and individual analysis uncertainties are 2σ , represented by ellipse size.

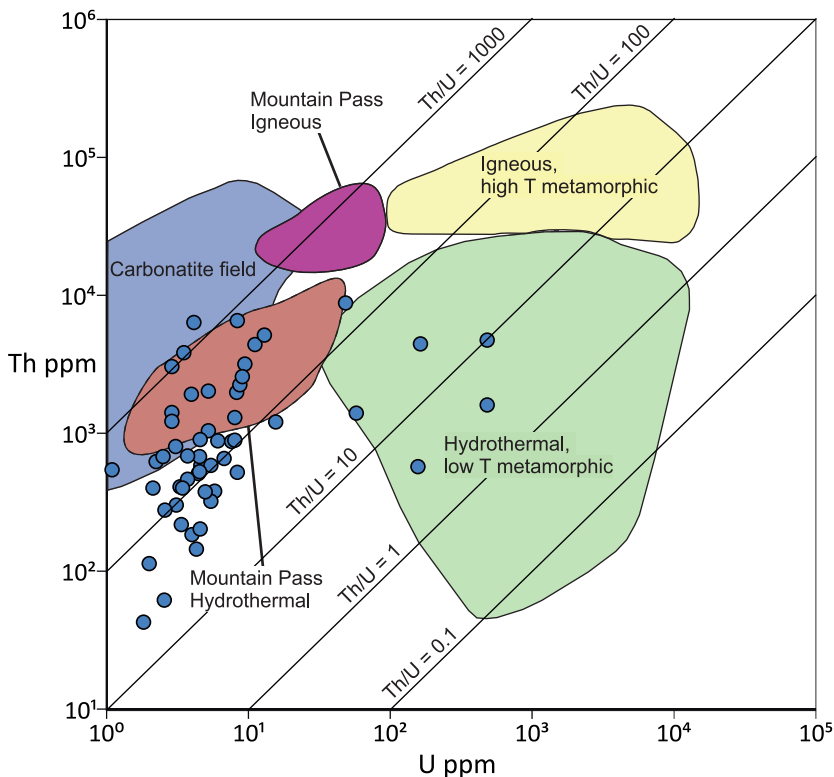


Figure 3. Monazite U versus Th diagram. The analyzed monazite (blue circles) are dispersed and plot mostly to the carbonatite and Mountain Pass hydrothermal fields or below them. Most analyses are situated in the low U area with 100–1000 Th/U. Some analyses have atypically low Th and plot outside of all compositional fields. ‘Igneous and high T metamorphic’, ‘hydrothermal and low T metamorphic’, and ‘carbonatite fields’ are from Zi et al (2024). Mountain Pass monazite fields are based on Figure 17b in Benson & Watts (2024). Both axes are logarithmic.

alteration at ~ 1760 Ma. The monazite U-Pb system can be reset below its closure temperature by fluid mediated coupled dissolution-precipitation (Harlov et al. 2011; Williams et al. 2011; Budzyń et al. 2021b). Fluid-interaction should modify the BSE signal in monazite compared to unaltered areas, due to either lower (Williams et al. 2011) or higher (Shazia et al. 2015) concentrations of high Z elements (i.e., Th, Pb, and U) in the altered areas, resulting in darker or brighter BSE signals, respectively. Neither zonation nor heterogeneity were observed during BSE imaging of any of the monazite grains analyzed in this study (Fig. 1; Electronic appendix A). Fluid-induced alteration will also lead to lower Th content, and consequently, lower Th/U. The conspicuous systematic textural association of apatite and monazite, however, is not explained by metasomatic alteration of primary monazite.

The studied monazite has low U and Th content, compared to typical monazite (e.g., Zi et al. 2024; Fig. 3). Carbonatitic monazite also typically has low U (<100 ppm) and elevated Th/U (>1000 , Zi et al. 2024). The studied monazite generally plot in and below the carbonatite field (Fig. 3), due to the low Th content, and in the field of hydrothermal monazite from the Mountain Pass carbonatite (Benson & Watts 2024). The atypically low Th and U content of the monazite analyzed in this study can be explained as inherited from the apatite, which has very low content of both elements (<4 ppm and <20 ppm, respectively) but highly varying Th/U ratios (3–184, Karvinen et al. 2024). The analyzed monazite has been previously interpreted as metasomatic (Karvinen et al. 2024), based on its textural association with two generations of apatite — large (>1000 μm) apatite with fluid and mineral inclusions and fine-grained (<100 μm), recrystallized apatite devoid of inclusions (Fig. 1; Fig. 5 in Karvinen et al. 2024). Interaction of apatite and hydrothermal fluids may lead to complex dissolution and reprecipitation processes of apatite and to the formation of monazite (e.g., Harlov et al. 2005 and references therein). This process has been invoked to explain textural relationships found in natural rocks between apatite and monazite where

monazite is within, in contact or near apatite, a common observation in carbonatites (e.g., Chen et al. 2017; Lu et al. 2021; Su et al. 2021). Therefore, we conclude that the monazite analyzed in this study is post-magmatic and metasomatic in origin, and the 1760 ± 17 Ma lower concordia intercept is our best estimate for the minimum age for the apatite-fluid processes that formed the monazite.

5.2 1780–1760 Ma monazite in the northern Fennoscandian shield

Ages similar to the age result presented above are found within the youngest monazite age populations elsewhere in northern Fennoscandia (~ 1780 – 1760 Ma; Corfu & Evins 2002; Lahtinen et al. 2013; Hölttä et al. 2020; Salminen et al. 2022) that experienced metamorphic overprint in the Svecofennian orogeny (Hölttä & Heilimo 2017). The orogeny was followed by a large-scale orogenic collapse at 1790–1770 Ma (Lahtinen et al. 2005), before crustal stabilization after 1760 Ma (Nironen 2017). In the Raahe-Ladoga shear zone, metamorphic monazite, formed through dissolution-reprecipitation processes from apatite, was dated at 1793 ± 3 Ma, interpreted to represent recrystallization related to the final stage of Svecofennian deformation (Woodard et al. 2017). In northern Fennoscandia, monazite within the Central Lapland Granitoid Complex yields a similar U-Pb age (1785 ± 9 Ma) likewise interpreted to represent the final deformation stage associated with compressional shortening at 1780–1760 Ma, followed by retrogressive metamorphism (Lahtinen et al. 2018). This metamorphic overprint also affected zircon, the youngest metamorphic rims yield ages of ca. 1760 Ma (Lahtinen et al. 2018).

Similar ages are also reported from within the Siilinjärvi complex from other isotope systems and minerals (2030–1770 Ma; K-Ar, Puustinen 1972; Rb-Sr, Tichomirowa et al. 2006; this study) and elsewhere in the Archean craton in eastern Finland (1795 ± 21 Ma, K-Ar in biotite; Kontinen et al. 1992). The ca. 1800–1770 Ma monazite dates from paragneisses from the Svecofennian province in

Central Finland were primarily from monazite rims and overgrowths, indicating secondary monazite growth likely due to dissolution-precipitation processes (Salminen et al. 2022), as discussed previously. Monazite from metasedimentary rocks in the Karelia province primarily yields ages of 1790–1770 Ma (Hölttä et al. 2020 and references therein). The metamorphic monazite ages overlap with the age presented in this study. The difference between the fluid-mineral reactions was likely controlled by the rock composition, as apatite is abundant in the Siilinjärvi complex, and only an accessory phase in typical paragneisses. In this study, monazite was formed from interaction between apatite and hydrothermal fluids, rather than monazite-fluid reactions or solid-state metamorphic growth.

Conclusions

This study reports the first U-Pb dating result of monazite from the Neoproterozoic Siilinjärvi glimmerite-carbonatite complex. The lower concordia intercept age of 1760 ± 17 Ma (2σ) shows that the monazite, at least in the studied sample, is post-magmatic, metasomatic in origin and formed through dissolution-precipitation reactions between hydrous fluid and apatite. This study provides temporal information about the flux of hydrothermal fluids in the Archean bedrock in the Karelia province and gives a minimum age for post-orogenic fluid-rock interactions at the onset of cratonization of the Fennoscandian shield.

Acknowledgements

K.H. Renlund Foundation is acknowledged for funding the PhD thesis project of the first author. Kieran Iles and Evgenia Salin are thanked for thoughtful reviews that improved the manuscript. Jussi Heinonen is additionally thanked for providing valuable feedback on a previous draft of this manuscript. We acknowledge Mikko Savolainen, formerly of Yara Suomi Oy, for providing the sample.

Authorship contribution statement

S. Karvinen – Conceptualization, analytical work, data reduction, interpretation, writing; K. Cutts – analytical work, data reduction, interpretation, editing; H. O’Brien – analytical work, data reduction, interpretation, editing; C. Beier – editing, supervision; A. Heinonen – editing, supervision.

Supplementary data

Supplementary data for this article is available via Zenodo data repository: <https://doi.org/10.5281/zenodo.18754428> (Karvinen et al. 2026)

References

- Al-Ani, T. 2013. Mineralogy and Petrography of Siilinjärvi Carbonatite and Glimmerite Rocks, Eastern Finland. Geological Survey of Finland Report 164. Available online: <https://hakku.gtk.fi/en/publications?id=19554>
- Benson, E.K. & Watts, K.E., 2024. Apatite and Monazite Geochemistry Record Magmatic and Metasomatic Processes in Rare Earth Element Mineralization at Mountain Pass, California. *Economic Geology* 119, 1611–1642. <https://doi.org/10.5382/econgeo.5108>
- Budzyń, B., Harlov, D. E., Williams, M. L., & Jercinovic, M. J., 2011. Experimental determination of stability relations between monazite, fluorapatite, allanite, and REE-epidote as a function of pressure, temperature, and fluid composition. *American Mineralogist* 96, 1547–1567. <https://doi.org/10.2138/am.2011.3741>
- Budzyń, B., Sláma, J., Corfu, F., Crowley, J., Schmitz, M., Williams, M.L., Jercinovic, M.J., Kozub-Budzyń, G.A., Konečný, P., Rzepa, G. & Włodek, A., 2021a. TS-Mnz – A new monazite age reference material for U-Th-Pb microanalysis. *Chemical Geology* 572, 120195. <https://doi.org/10.1016/j.chemgeo.2021.120195>
- Budzyń, B., Wirth, R., Sláma, J., Birski, Ł., Tramm, F., Kozub-Budzyń, G.A., Rzepa, G. & Schreiber, A., 2021b. LA-ICPMS, TEM and Raman study of radiation damage, fluid-induced alteration and disturbance of U-Pb and Th-Pb ages in experimentally metasomatized monazite. *Chemical Geology* 583, 120464. <https://doi.org/10.1016/j.chemgeo.2021.120464>
- Chen, W., Honghui, H., Bai, T. & Jiang, S., 2017. Geochemistry of Monazite within Carbonatite Related

- REE Deposits. *Resources* 6, 51. <https://doi.org/10.3390/resources6040051>
- Cherniak, D.J., Watson, E.B., Grove, M. & Harrison, T.M., 2004. Pb diffusion in monazite: a combined RBS/SIMS study. *Geochimica et Cosmochimica Acta* 68, 829–840. <https://doi.org/10.1016/j.gca.2003.07.012>
- Chew, D.M., Petrus, J.A. & Kamber, B.S., 2014. U–Pb LA–ICP–MS dating using accessory mineral standards with variable common Pb. *Chemical Geology* 363, 185–199. <https://doi.org/10.1016/j.chemgeo.2013.11.006>
- Corfu, F. & Evins, P.M., 2002. Late Palaeoproterozoic monazite and titanite U–Pb ages in the Archaean Suomijärvi Complex, N-Finland. *Precambrian Research* 116, 171–181. [https://doi.org/10.1016/S0301-9268\(02\)00024-4](https://doi.org/10.1016/S0301-9268(02)00024-4)
- Harlov, D.E., Wirth, R. & Förster, H.-J., 2005. An experimental study of dissolution–reprecipitation in fluorapatite: fluid infiltration and the formation of monazite. *Contributions to Mineralogy and Petrology* 150, 268–286. <https://doi.org/10.1007/s00410-005-0017-8>
- Harlov, D.E., 2015. Apatite: A Fingerprint for Metasomatic Processes. *Elements* 11, 171–176. <https://doi.org/10.2113/gselements.11.3.171>
- Harlov, D.E., Wirth, R. & Hetherington, C.J., 2011. Fluid-mediated partial alteration in monazite: the role of coupled dissolution–reprecipitation in element redistribution and mass transfer. *Contributions to Mineralogy and Petrology* 162, 329–348. <https://doi.org/10.1007/s00410-010-0599-7>
- Högltrå, P., Huhma, H., Mänttari, I., & Paavola, J., 2000. P–T development of Archaean granulites in Varpaisjärvi, central Finland. II. Dating of high-grade metamorphism with the U–Pb and Sm–Nd methods: *Lithos* 50, 121–136. [https://doi.org/10.1016/S0024-4937\(99\)00055-9](https://doi.org/10.1016/S0024-4937(99)00055-9)
- Högltrå, P. & Heilimo, E. 2017. Metamorphic map of Finland. In: Nironen, M. (ed.) *Bedrock of Finland at the scale 1:1 000 000 – Major stratigraphic units, metamorphism and tectonic evolution*. Geological Survey of Finland, Special Paper 60, 77–128. Available online: <https://hakku.gtk.fi/en/publications?id=21191>
- Högltrå, P., Huhma, H., Lahaye, Y., Mänttari, I., Lukkari, S. & O'Brien, H., 2020. Paleoproterozoic metamorphism in the northern Fennoscandian Shield: age constraints revealed by monazite. *International Geology Review* 62, 360–387. <https://doi.org/10.1080/00206814.2019.1611488>
- Karvinen, S., Heinonen, A., Beier, C. & Jöns, N., 2024. The composition of apatite in the Archaean Siilinjärvi glimmerite-carbonatite complex in eastern Finland. *Bulletin of the Geological Society of Finland* 96, 5–34. <https://doi.org/10.17741/bgsf/96.1.001>
- Karvinen, S., Cutts, K., O'Brien, H., Beier, C., & Heinonen, A., 2026. Electronic appendices to 'Metasomatic monazite growth as a result of apatite-fluid interactions: U–Pb dating of monazite in the Siilinjärvi glimmerite-carbonatite complex, Finland' [Data set]. Zenodo. <https://doi.org/10.5281/zenodo.18754428>
- Kohonen, J., Lahtinen, R., Luukas, J. & Nironen, M., 2021. Classification of regional-scale tectonic map units in Finland. *Developments in map data management and geological unit nomenclature in Finland*. Geological Survey of Finland, Bulletin 412, 33–80. <https://doi.org/10.30440/bt412.2>
- Kontinen, A., Paavola, J. & Lukkari, H., 1992. K–Ar ages of hornblende and biotite from Late Archaean rocks of eastern Finland - interpretation and discussion of tectonic implications. *Bulletin de la Commission Géologique de Finlande* 365. 31 p. Available online: <https://hakku.gtk.fi/en/publications?id=263>
- Korsman, K., Korja, T., Pajunen, M., Virransalo, P. & Ggt/Sveka Working Group, 1999. The GGT/SVEKA Transect: Structure and Evolution of the Continental Crust in the Paleoproterozoic Svecofennian Orogen in Finland. *International Geology Review* 41, 287–333. <https://doi.org/10.1080/00206819909465144>
- Lahtinen, R., Korja, A. & Nironen, M., 2005. Chapter 11 Paleoproterozoic tectonic evolution. In: Lehtinen, M., Nurmi, P.A. & Rämö, O.T. (eds.) *Precambrian Geology of Finland – Key to the Evolution of the Fennoscandian Shield*. *Developments in Precambrian Geology* 14, Elsevier, pp. 481–531. [https://doi.org/10.1016/S0166-2635\(05\)80012-X](https://doi.org/10.1016/S0166-2635(05)80012-X)
- Lahtinen, R., Huhma, H., Lahaye, Y., Kontinen, A., Kohonen, J. & Johanson, B., 2013. Long-lived LREE mobility in the cratonic, rift and foredeep to foreland sedimentary cover at the western margin of the Karelia Province. *Lithos* 175–176, 86–103. <https://doi.org/10.1016/j.lithos.2013.05.003>
- Lahtinen, R., Huhma, H., Lahaye, Y., Lode, S., Heinonen, S., Sayab, M. & Whitehouse, M.J., 2016. Paleoproterozoic magmatism across the Archean-Proterozoic boundary in central Fennoscandia: Geochronology, geochemistry and isotopic data (Sm–Nd, Lu–Hf, O). *Lithos* 262, 507–525. <https://doi.org/10.1016/j.lithos.2016.07.014>
- Lahtinen, R., Huhma, H., Sayab, M., Lauri, L.S. & Högltrå, P., 2018. Age and structural constraints on the tectonic evolution of the Paleoproterozoic Central Lapland Granitoid Complex in the Fennoscandian Shield. *Tectonophysics* 745, 305–325. <https://doi.org/10.1016/j.tecto.2018.08.016>
- Lu, J., Chen, W., Ying, Y., Jiang, S. & Zhao, K., 2021. Apatite texture and trace element chemistry of carbonatite-related REE deposits in China: Implications for petrogenesis. *Lithos* 398–399, 106276. <https://doi.org/10.1016/j.lithos.2021.106276>
- Lukkari, H., 2008. Geological map of Finland 1:100 000 Explanation to the maps of pre-quaternary rocks, sheets 3331 and 3242. Available online: <https://hakku.gtk.fi/en/publications?id=2954>
- Mazoz, A., Gonçalves, G.O., Lana, C., Buick, I.S., McSwiggen, P.L., Corfu, F., Kamo, S.L., Fu, B., Wang, H., Moreira, H., Scholz, R., Martins, L., Peixoto, E., Dantas, E.L. & Santos, R.V., 2024. Vermilion monazite: A new

- Archean reference material for U-Pb and Sm-Nd microanalysis. *Chemical Geology* 658, 122121. <https://doi.org/10.1016/j.chemgeo.2024.122121>
- Molnár, F., Middleton, A., Stein, H., O'Brien, H., Lahaye, Y., Huhma, H., Pakkanen, L. & Johanson, B., 2018. Repeated syn- and post-orogenic gold mineralization events between 1.92 and 1.76 Ga along the Kiistala Shear Zone in the Central Lapland Greenstone Belt, northern Finland. *Ore Geology Reviews* 101, 936–959. <https://doi.org/10.1016/j.oregeorev.2018.08.015>
- Nironen, M. (Ed.), 2017. Bedrock of Finland at the scale 1:1 000 000 - major stratigraphic units, metamorphism and tectonic evolution, Special paper / Geological Survey of Finland. Geological Survey of Finland, Espoo. Available online: <https://hakku.gtk.fi/en/publications?id=21191>
- O'Brien, H., Heilimo, E. & Heino, P., 2015. The Archean Siilinjärvi Carbonatite Complex. In: Maier, W.D., Lahtinen, R. & O'Brien, H. (eds.), *Mineral Deposits of Finland*. Elsevier, pp. 327–343. <https://doi.org/10.1016/B978-0-12-410438-9.00013-3>
- Paton, C., Hellstrom, J., Paul, B., Woodhead, J., Hergt, J., 2011. Iolite: Freeware for the visualisation and processing of mass spectrometric data. *Journal of Analytical Atomic Spectrometry* 26, 2508–2518. <https://doi.org/10.1039/c1ja10172b>
- Petrus, J. A., & Kamber, B. S., 2012. VizualAge: A Novel Approach to Laser Ablation ICP-MS U-Pb Geochronology Data Reduction. *Geostandards and Geoanalytical Research* 36, 247–270. <https://doi.org/10.1111/j.1751-908X.2012.00158.x>
- Puustinen, K., 1971. Geology of the Siilinjärvi carbonatite complex, Eastern Finland. *Bulletin de la Commission Géologique de Finlande* 249, 43 pages. Available online: <https://hakku.gtk.fi/en/publications?id=469>
- Puustinen, K., 1972. Richterite and actinolite from the Siilinjärvi carbonatite complex, Finland. *Bulletin of the Geological Society of Finland* 44, 83–86. <https://doi.org/10.17741/bgsf/44.1.007>
- Rukhlov, A.S. & Bell, K., 2010. Geochronology of carbonatites from the Canadian and Baltic Shields, and the Canadian Cordillera: clues to mantle evolution. *Mineralogy and Petrology* 98, 11–54. <https://doi.org/10.1007/s00710-009-0054-5>
- Salminen, P.E., Hölttä, P., Lahtinen, R. & Sayab, M., 2022. Monazite record for the Paleoproterozoic Svecofennian orogeny, SE Finland: An over 150-Ma spread of monazite dates. *Lithos* 416–417, 106654. <https://doi.org/10.1016/j.lithos.2022.106654>
- Sartori, G., Galli, A., Weidendorfer, D. & Schmidt, M.W., 2022. A tool to distinguish magmatic from secondarily recrystallized carbonatites—Calcite/apatite rare earth element partitioning. *Geology* 51, 54–58. <https://doi.org/10.1130/G50416.1>
- Schoene, B., 2014. U–Th–Pb Geochronology. In: Holland, H. D. & Turekian, K.K. (eds.), *Treatise on Geochemistry*. Elsevier Science, pp. 341–378. <https://doi.org/10.1016/B978-0-08-095975-7.00310-7>
- Shazia, J.R., Harlov, D.E., Suzuki, K., Kim, S.W., Girish-Kumar, M., Hayasaka, Y., Ishwar-Kumar, C., Windley, B.F. & Sajeev, K., 2015. Linking monazite geochronology with fluid infiltration and metamorphic histories: Nature and experiment. *Lithos* 236–237, 1–15. <https://doi.org/10.1016/j.lithos.2015.08.008>
- Su, J.-H., Zhao, X.-F., Li, X.-C., Su, Z.-K., Liu, R., Qin, Z.-J., & Chen, M., 2021. Fingerprinting REE mineralization and hydrothermal remobilization history of the carbonatite-alkaline complexes, Central China: Constraints from in situ elemental and isotopic analyses of phosphate minerals. *American Mineralogist* 106, 1545–1558. <https://doi.org/10.2138/am-2021-7746>
- Tichomirowa, M., Grosche, G., Gotze, J., Belyatsky, B., Savva, E., Keller, J. & Todt, W., 2006. The mineral isotope composition of two Precambrian carbonatite complexes from the Kola Alkaline Province – Alteration versus primary magmatic signatures. *Lithos* 91, 229–249. <https://doi.org/10.1016/j.lithos.2006.03.019>
- Vermeesch, P., 2018. IsoplotR: A free and open toolbox for geochronology. *Geoscience Frontiers* 9, 1479–1493. <https://doi.org/10.1016/j.gsf.2018.04.001>
- Williams, I.S., Buick, I.S. & Cartwright, I., 1996. An extended episode of early Mesoproterozoic metamorphic fluid flow in the Reynolds Range, central Australia. *Journal of Metamorphic Geology* 14, 29–47. <https://doi.org/10.1111/j.1525-1314.1996.00029.x>
- Williams, M.L., Jercinovic, M.J. & Hetherington, C.J., 2007. Microprobe Monazite Geochronology: Understanding Geologic Processes by Integrating Composition and Chronology. *Annual Review of Earth and Planetary Sciences* 35, 137–175. <https://doi.org/10.1146/annurev.earth.35.031306.140228>
- Williams, M.L., Jercinovic, M.J., Harlov, D.E., Budzyń, B. & Hetherington, C.J., 2011. Resetting monazite ages during fluid-related alteration. *Chemical Geology* 283, 218–225. <https://doi.org/10.1016/j.chemgeo.2011.01.019>
- Woodard, J., Tuisku, P., Kärki, A., Lahaye, Y., Majka, J., Huhma, H. & Whitehouse, M.J., 2017. Zircon and monazite geochronology of deformation in the Pielavesi Shear Zone, Finland: multistage evolution of the Archaean–Proterozoic boundary in the Fennoscandian Shield. *Journal of the Geological Society* 174, 255–267. <https://doi.org/10.1144/jgs2016-020>
- Yardley, B.W.D., 2013. The Chemical Composition of Metasomatic Fluids in the Crust. In: Harlov, E. & Austrheim, H. (eds.), *Metasomatism and the chemical transformation of Rock: The role of fluids in terrestrial and extraterrestrial processes*. Springer, Berlin, Heidelberg, pp. 17–51. https://doi.org/10.1007/978-3-642-28394-9_2
- Zi, J.-W., Muhling, J. R., & Rasmussen, B., 2024. Geochemistry of low-temperature (<350 °C) metamorphic and hydrothermal monazite. *Earth-Science Reviews* 249, 104668. <https://doi.org/10.1016/j.earscirev.2023.104668>